Jpn. J. Appl. Phys. Vol. 42 (2003) pp. 5753–5758
Part 1, No. 9A, September 2003

Characterization of a Pulse-Charge-Mode Multigap Pseudospark Device as an Enhanced Electron Beam Source

Yong Kon KWON*, S. H. NAM[1], Eui Wan LEE, Soung Soo PARK[1] and Yeong Jin HAN[1]

Department of Physics, Kyungpook National University, Daegu 702-701, Korea
[1]*Pohang Accelerator Laboratory, POSTECH, Pohang 790-784, Korea*

(Received January 17, 2003; accepted for publication May 9, 2003)

Multigap pseudospark devices can be used to produce intense pulsed electron beams. Pseudospark discharge is generally initiated by self-breakdown or an external trigger in which DC high voltage is used. In this work, we investigated a pulse charge mode to generate an enhanced pulsed electron beam from a 10-gap pseudospark device. In the pulse charge mode, pulsed high voltage is applied to the device. Using the pulse charge mode, we could obtain enhanced electron beams in wider ranges of voltage and pressure than in the self-discharge or the trigger mode. We achived a maximum efficiency of enhanced electron beams at 3×10^{-1} mbar of Ar gas. Under this best pressure condition, we also observed well-focused electron beams with a diameter of down to 0.1 mm, peak current of up to 130 A, and full width at half maximum (FWHM) of 10 ns. The peak power density was 10^{10} W/cm^2. [DOI: 10.1143/JJAP.42.5753]

KEYWORDS: pulse charge mode, electron beam, pseudospark discharge, multigap pseudospark devices, peak power density

1. Introduction

The pseudospark structure was first developed as a particle beam source by Christiansen and Schultheiß in 1978.[1)] Intense electron and ion beams can be simultaneously produced for a very short time in opposite directions of the pseudospark discharge chamber.[2)] The electron beams produced in pseudospark discharge show a self-focusing characteristic without an external focusing magnetic field. The self-focusing of the beam is believed to occur because of space charge neutralization.[3)] A main advantage of the pseudospark-produced beams is high peak current while maintaining a good beam emittance characteristic. The pseudospark-produced electron beam has received considerable attention in the last several years because of its applicability in various areas, such as those of free-electron lasers,[4)] material processing,[5)] and point sources of soft X-rays.[6)] Furthermore, due to the high power density of the electron beam at the target surface (10^9–10^{12} W/cm^2), the electron beam can evaporate materials that have a high melting point or very complex stoichiometric structure. Hence, by electron beam ablation, it could be possible to prepare thin films such as high-temperature-superconducting thin films of $YBa_2Cu_3O_{7-x}$[7)] and metal thin films.[8)] The beam power is comparable to those of pulsed high-power lasers that are commonly used in thin film production.[9)] In addition to the pulsed intense beam source application, the pseudospark discharge can be applied in various other areas, such as that of a high power switch,[10)] because of its high-density uniform-plasma generation.

To produce uniform glow discharge, the pseudospark device generally follows the left branch of the Paschen curve with the internal gas pressure ranging from 1×10^{-2} to 5×10^{-1} mbar depending on the device structure. The working gases are commonly air, N_2, H_2, O_2, and noble gases.[11)] There are two generally known methods of producing the pseudospark discharge: self-discharge and the external trigger.[12,13)] In the self-discharge mode, the discharge is produced by gradually increasing the applied gap voltage with a fixed internal gas pressure or vice versa. In the external trigger mode, the discharge is initiated by an externally applied high-voltage trigger pulse. The trigger pulse produces a seed plasma and leads to the main discharge in the pseudospark device which is filled with a certain gas and has an external energy storage device. The internal gas pressure and the electrode gap distance determine the self-discharge voltage. Therefore, for a fixed gap distance and internal gas pressure, the allowable applied voltage in the trigger mode is lower than that in the self-discharge mode. In other words, we cannot raise the applied voltage higher than the self-discharge voltage.

In order to overcome the self-discharge voltage limitation, we adopted a new pulse charge mode for the pseudospark electron beam source. In the pulse charge mode, the pseudospark device sees the high voltage as a pulse, rather than DC that is common in self-discharge and trigger modes. By adopting the pulse charge mode, we can apply a much higher voltage than that which is limited by the self-breakdown characteristic of the device. Such a method can produce more intense electron beams. The results of a detailed study on the pulse-charge-mode pseudospark electron beam source are described here. The device used in this work is a 10-gap pseudospark device. The multigap pseudospark device has been commonly used in many electron beam generation experiments to improve the intensity and collimation of the extracted electron beams.[12,14)]

The pseudospark discharge is known to have five characteristic phases.[15,16)] When the plasma produced by the external trigger enters into the hollow cathode region during phase I , pendulum electrons and photoemission lead to very efficient multiplication of the charge carriers in phase II, which is called the hollow cathode phase. The current increases in strength to several hundred amperes and the voltage drops to several hundreds of volts during the hollow cathode phase. The high-density electrons are emitted to the main gap, and the current increases to 10^5 A and above with a high current rise rate of 10^{12} A/s during phase III, which is the bore hole phase. The discharge subsequently develops to the high-current and metal vapor arc phases. The final phase is governed by the amount of external storage energy. From phase III, the hollow cathode does not have its original

*E-mail: kwonyk@postech.ac.kr

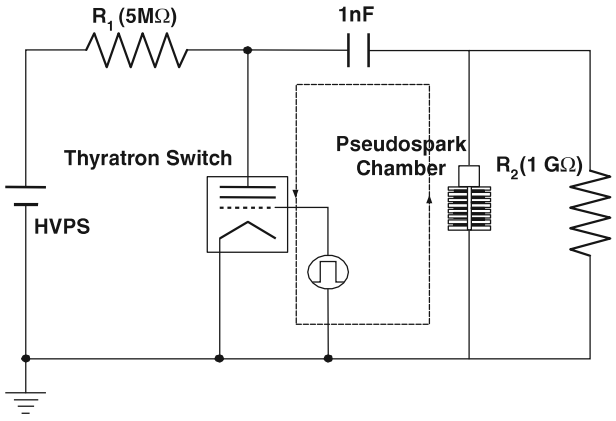

Fig. 1. Schematic electrical test circuit diagram of a pulse-charge-mode multigap pseudospark system. (arrow: discharge current path)

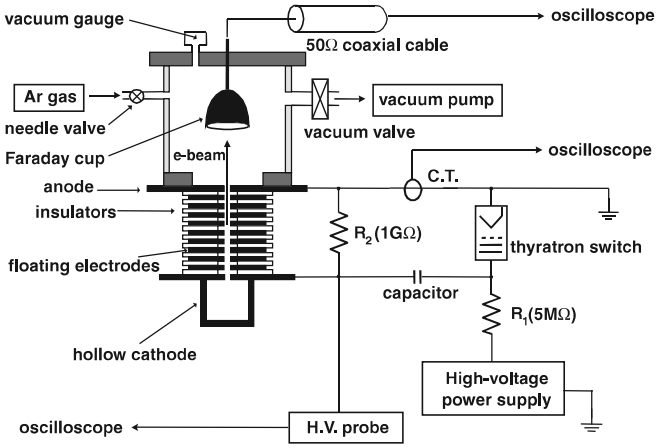

Fig. 2. Schematic drawing of measurement setup in a pulse-charge-mode multigap pseudospark system.

function. Instead, the cathode functions as a normal plane electrode. The electron beam extracted from the anode can thus be obtained only before phase III. Excess energy provided after phase II is not efficiently involved in the generation of electron beams, and moreover, it forms the main current that flows between the main electrodes. For the application of electron beam extraction, the main current flow should be minimized to reduce electrode wear and thus maximize the system reliability and lifetime.

2. Experimental Setup

2.1 Electrical circuit

Figure 1 shows the schematic test circuit diagram of the pulse-charge-mode pseudospark experiment. The system consisted of a DC high-voltage power supply, energy storage capacitors, charging resistors, a pseudospark chamber, and a thyratron switch. The energy was charged to the 1 nF capacitor bank from the positive 50 kV power supply via 5 MΩ and 1 GΩ charging resistors. The capacitor bank consisted of eight 500 pF capacitors that were connected in series and parallel to form 1 nF. In order to efficiently extract the electron beam while minimizing the main current, we should concentrate on device operation in the hollow cathode phase (phase II).[17] Therefore, we chose the 1 nF capacitance.[18] Minimizing the main current will reduce electrode erosion and thus maximize the device lifetime. The capacitors were closely positioned near the cathode and radially distributed around the cathode to produce uniform discharge.

After charging, the thyratron switch was triggered to induce negative pulsed high voltage across the pseudospark device. The pseudospark chamber was filled with gas at the appropriate pressure to induce breakdown with the pulsed high voltage applied after the thyratron trigger. The method illustrated in Fig. 1 is here called the pulse-charge-mode method. In the pulse charge mode, there is a certain delay from the time of high-voltage application to the time of breakdown. By using the delay characteristic, we can apply a voltage higher than the self-discharge voltage. Therefore, we can significantly extend the operation voltage range of the pseudospark device with the pulse charge mode.

2.2 Measurement setup

Figure 2 shows the experimental setup of the multigap pseudospark device. The pseudospark device had a 10-gap structure with a hollow cathode. It had nine floating electrodes and ten insulators that were stacked alternately between the anode and the hollow cathode. A drift chamber was mounted on top of the anode to install a Faraday cup, a vacuum gauge, a gas inlet valve, and a vacuum pump. A glass cylinder was used for the drift chamber. Gas inlet and vacuum pump ports were mounted on the insulated glass drift chamber. The hollow cathode cavity was made of brass, and its height and diameter were 50 mm and 40 mm, respectively. The donut-shaped disk anode was made of 22-mm-thick aluminum with 270 mm outer and 4 mm inner diameters. Floating electrodes were made of brass with a thickness of 5 mm. Outer and inner diameters of the floating electrodes were 64 mm and 4 mm, respectively. Insulators were made of glass that had a thickness of 5 mm, and outer and inner diameters of 100 and 25 mm, respectively.

Voltage generated across the pseudospark device was measured with a Tektronix P6015A high-voltage probe, and the main discharge current was measured with a Pearson current transformer (CT). The electron beam was measured with a Faraday cup. The Faraday cup was conical and placed 20 mm above the anode center hole. As mentioned, a fixed 1 nF capacitor bank was used as an energy storage device. The chamber pressure was varied from 2×10^{-2} mbar to 50 mbar of Ar gas.

3. Experimental Results and Discussion

Figure 3 shows plots of gas pressure versus breakdown voltage of the 10-gap pseudospark device. In the figure, there are three plots for the calculations for the self-discharge mode, experimental results for the self-discharge mode, and experimental results for the pulse charge mode. The empirical formula used for the calculated self-discharge mode is[19]

$$V_b = \frac{2.0}{(P^2 dD)^2}, \tag{3.1}$$

where V_b is the self-discharge voltage in volts, P is the gas pressure in Torr, d is the distance between the anode and the

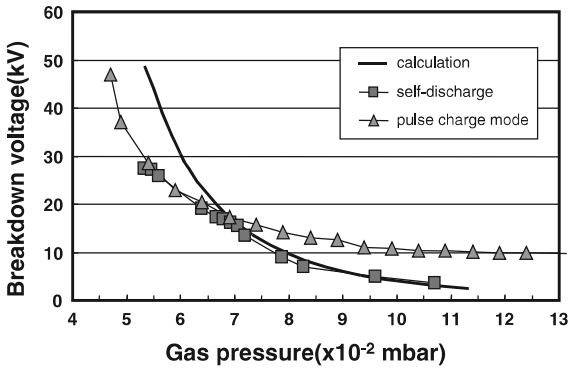

Fig. 3. Plots of breakdown voltage versus internal gas pressure.

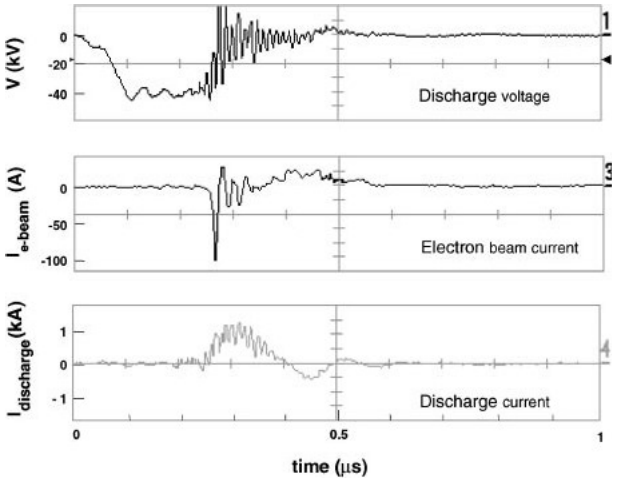

Fig. 4. Typical oscillograms of voltage, electron beam current and main discharge current of the 10-gap pseudospark device in the pulse charge mode. Charging voltage: 40 kV; Peak pulse voltage: 39 kV; Peak electron beam current: 110 A; Ar gas pressure: 5×10^{-1} mbar; Discharge delay time: 260 ns; Main discharge current peak: 1 kA.

cathode in cm, and D is the cathode hole diameter in cm. d and D in this experiment were 10 cm and 0.4 cm, respectively. Data obtained in the pulse charge mode represents the minimum voltage required to induce breakdown of the device. The minimum voltage was measured by slowly increasing the DC charging voltage of capacitors, while maintaining the internal gas pressure at a specific desired value, as well as the thyratron switch triggering rate at 1 Hz. The rise time of the pulse was about 60 ns. The discharge delay time, which was measured from the thyratron trigger to the instant of device breakdown, varied depending on the internal gas pressure, but was never less than the pulse rise time. As predicted by Paschen's law, all three plots show that breakdown voltage of the pseudospark device increases as the internal gas pressure decreases. Moreover, the three plots exhibit similar tendencies within an acceptable experimental error range. The only notable difference between plots is that the plot for the pulse charge mode is extended over a far greater pressure range than the other plots. We could measure the minimum breakdown voltage in the pulse charge mode with an internal pressure range of up to 20 mbar. In Fig. 3, only data up to 13×10^{-2} mbar are shown to enable easy comparison with other plots. The minimum breakdown voltages in the pulse charge mode above this pressure were neither reduced nor increased much and remained at about 9 to 10 kV. The minimum voltage measured in the high-pressure range from 13×10^{-2} to 20 mbar could be described as the minimum voltage required to form plasma in the hollow cathode of the pseudospark device.[15] In the self-discharge mode, the breakdown voltage was not measurable above 1.1×10^{-1} mbar because of instantaneous breakdown when the high-voltage power supply was turned on.

Figure 4 shows typical oscillograms of voltage, electron beam current, and main discharge current of the 10-gap pseudospark device in the pulse charge mode. The charging voltage of the capacitor bank was about 40 kV DC. The internal gas pressure was 5×10^{-1} mbar of Ar. The trigger timing of the oscillograms was synchronized with the thyratron trigger. When the thyratron switch was triggered, pulse voltage developed across the pseudospark device up to nearly the charging voltage of 40 kV with a rise time of 60 ns. After a certain delay time, breakdown occurred. At a very early stage of breakdown, we measured the electron beam current. As shown in Fig. 4, the pulsed peak breakdown voltage measured was 39 kV, the peak electron beam current was 110 A, and the peak main discharge current was 0.9 kA. The discharge delay time was about 260 ns as measured from the thyratron trigger to the time of breakdown.

The delay time varied as the internal gas pressure changed. Figure 5 gives the relationship between the internal gas pressure and the breakdown delay time. Two different DC charging voltages were tested to observe the charging voltage dependence. We can see that the delay time decreases as the internal gas pressure increases. The delay time also somewhat decreases as the charging voltage increases. However, the charging voltage effect is reduced as the internal gas pressure increases. The discharge delay time above 10×10^{-1} mbar up to 20 mbar was also measured, and it was not reduced, but saturated at around 100 ns. A typical formative time lag at phase I of the pseudospark discharge is known to be some ten nanoseconds. Phase II (hollow cathode phase) starts about 10 to several 100 ns after phase I.[15] Therefore, the pseudospark device requires a certain minimum delay time before the discharge event. In our experiment, the minimum delay time observed was about

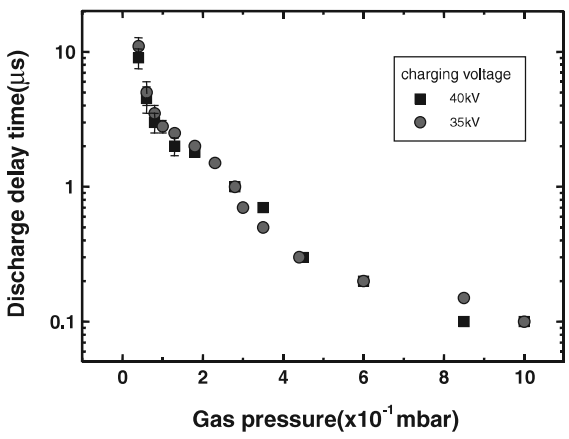

Fig. 5. Dependence of discharge delay time on Ar gas pressure for two different charging voltages.

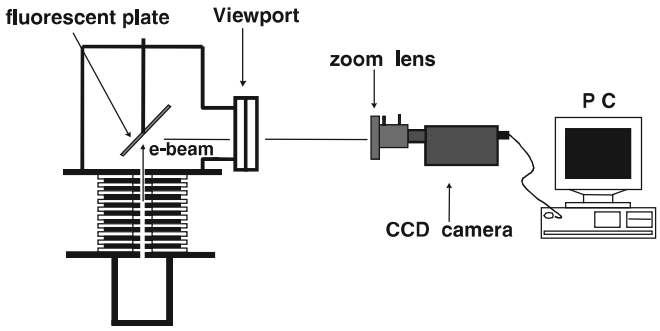

Fig. 6. Schematic drawing of the beam profile measurement setup.

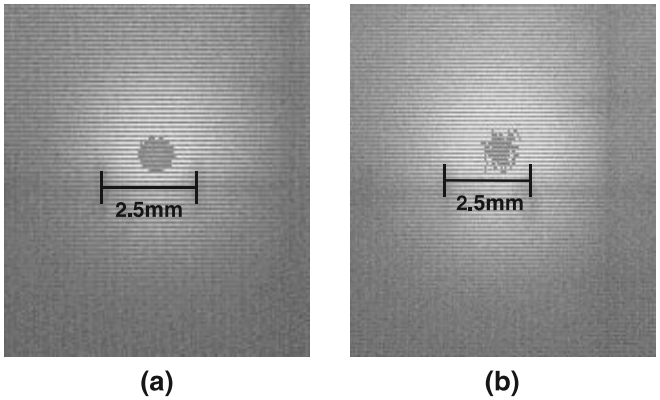

Fig. 8. Example images of focused and blurred electron beams. (a) 2.5×10^{-1} mbar of Ar; (b) 7×10^{-1} mbar of Ar.

100 ns, regardless of applied voltage or internal gas pressure. Therefore, considering the voltage pulse rise time of about 60 ns, the device always sees the DC charging voltage as the peak voltage before breakdown.

Figure 6 shows a schematic of the experimental setup used for measuring the electron beam profile. The electron beam extracted from the anode hole formed an image on the surface of a fluorescent plate that was aligned above 15 mm from the anode hole center. The profile of the electron beam was then digitally recorded and analyzed with a beam analyzer (Model LBA-300PC) that consisted of a CCD camera with a zoom lens and a beam analysis program. The beam analyzer reading corresponds to the radius of the electron beam within one standard deviation, σ, assuming a Gaussian beam distribution.[20] Figure 7 shows the variation of the beam diameter as a function of internal gas pressure, measured with a fixed discharge voltage of 38.5 kV. As shown, the beam diameter decreases as the internal gas pressure increases up to 3×10^{-1} mbar. The beam diameter then increases again above this pressure. The measured beam diameter ranges from 0.1 mm to 4 mm. Near 3×10^{-1} mbar, the beam is well focused. However, the beam is not well focused and becomes blurry at a pressure settings away from 3×10^{-1} mbar. Examples of images of focused and blurry beams are shown in Fig. 8. Figure 8(a) was measured with 2.5×10^{-1} mbar and (b) was measured with 7×10^{-1} mbar. The dark center in the figure represents the core of the beam and is the bright spot. The white area around the core is the part of the beam that has low beam density. The beam analyzer converted the beam image into a profile, and the beam size was measured from the beam profile. The measured beam diameters in Figs. 8(a) and 8(b) were 2.3 mm and 3.4 mm, respectively.

Peak electron beam current was measured as a function of peak discharge voltage and the results obtained for various gas pressures are shown Fig. 9. Measured peak electron beam current ranged from 35 to 130 A depending on experimental conditions. The peak electron beam current increased as the discharge voltage increased for a given internal gas pressure. From the figure, we can see that the controllable discharge voltage is very wide and ranges from 15 to 45 kV. For a given internal gas pressure, such wide voltage controllability is not realizable in the self-discharge or the trigger mode, but only possible in the pulse charge mode.

Measured peak electron beam current was also plotted as a function of internal gas pressure for various peak discharge voltages. The results are shown in Figs. 10 and 11. Internal Ar gas pressure was changed from 4×10^{-2} mbar to 20 mbar during the measurement. Figure 10 presents a plot of measurements in the pressure range from 4×10^{-2} to 6×10^{-1} mbar. As shown in Fig. 10, the maximum peak electron beam current was obtained at 3×10^{-1} mbar for all discharge voltage settings. At the pressure of 3×10^{-1} mbar, the beam was well focused, and the beam diameter became the smallest. The peak electron beam current started to

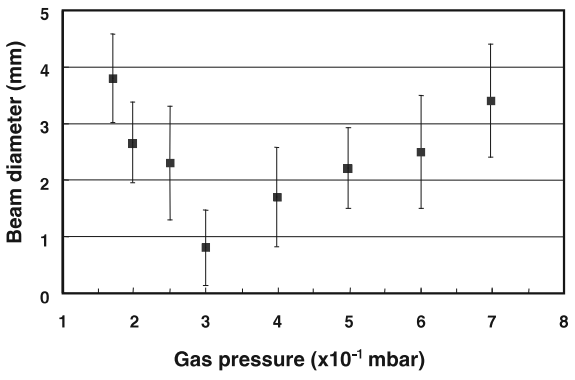

Fig. 7. Plot of electron beam diameter versus gas pressure. Pulse discharge voltage was 38.5 kV.

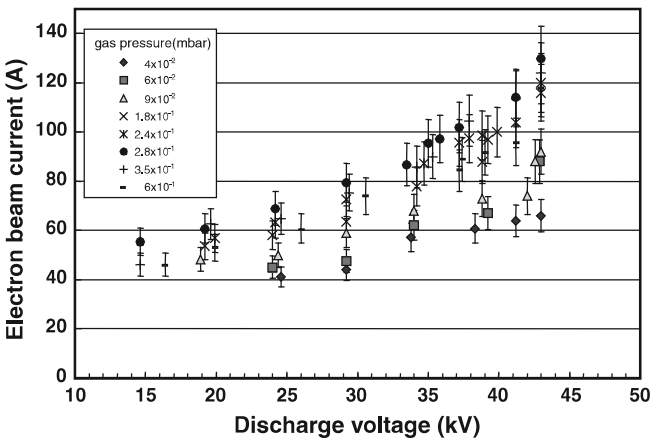

Fig. 9. Dependence of electron beam current on pulse discharge voltage for various Ar gas pressures.

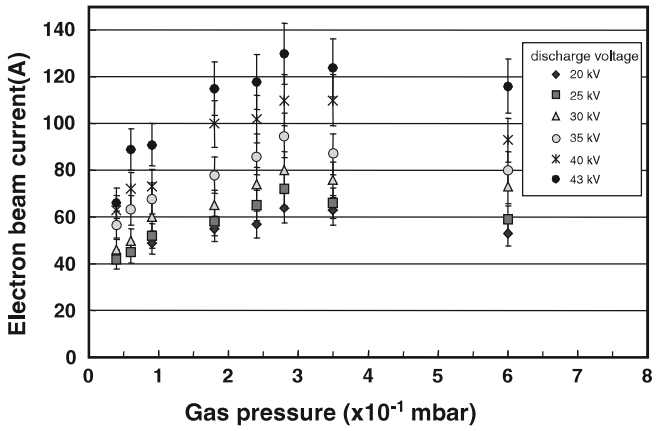

Fig. 10. Dependence of electron beam current on Ar gas pressure, ranging from 4×10^{-2} mbar to 6×10^{-1} mbar, for various discharge voltages.

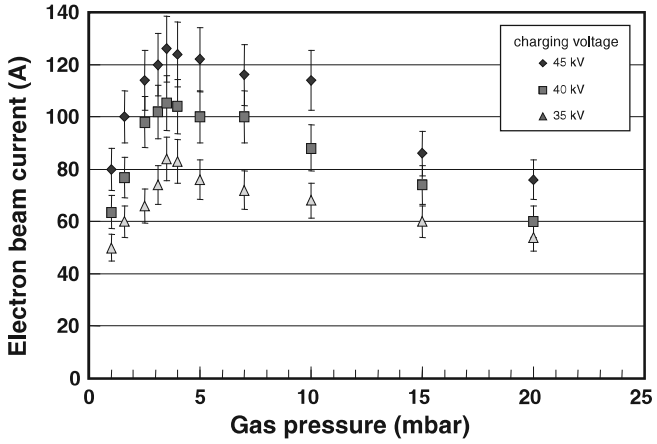

Fig. 11. Dependence of electron beam current on gas pressure, ranging from 1.0 mbar to 20 mbar, for various charging voltages.

decrease above 3×10^{-1} mbar. However, as shown Fig. 11, we found another peak of the electron beam current at around 3 mbar. Nevertheless, the beam was not as well focused as the one measured in 3×10^{-1} mbar. As described in previous sections, the discharge delay time was longer than the pulse rise time. Therefore, the electron energy gain in this pressure range would be comparable to that in other lower pressure ranges at a given charging voltage. We believe that the peak electron beam observed at 3×10^{-1} mbar was from runaway electrons that started from the hollow cathode.[15] This implies that the electrons produced at the hollow cathode reach the anode without further ionization due to the high electric field in the device gap. The maximum ionization cross section for electron impact of argon is at about 1 keV. In this mode, the electron beam propagated in a self-focused, space-charge-neutralized manner through the plasma channel and appeared as a well-focused beam at the anode output.[14] As the internal gas pressure increased, the probability of electron and gas atom interaction increased, and thus the accelerated electron energy would decrease. This process increased the ionization probability and thus the number of electrons in the device gap. These electrons would contribute to the increase of the measured peak electron beam current, but the beam that appeared was unfocused and blurry. For applications where a well-focused electron beam is required, the peak point at 3 mbar pressure may not as useful as the one obtained at 3×10^{-1} mbar. From the pressure versus electron beam measurement, we can again conclude that the pulse charge mode has a wide pressure range controllability than the self-discharge or the trigger mode.

The FWHM of the electron beam signal was also measured and found to range from 7 to 70 ns. Maximum power density of the electron beam was obtained as about 10^{10} W/cm^2 using the peak electron beam current of 120 A, FWHM of 10 ns, and beam diameter of 0.1 mm at 3×10^{-1} mbar. The power density obtained from the pseudospark device is comparable to the power density produced in excimer lasers for pulsed laser deposition (PLD) systems ($>10^9$ W/cm^2).[16] However, the cost and size of the pseudospark system could be much less than those of the laser PLD system. The operational repetition rate of the pseudospark system could reach several kHz. The minimum current density of the pseudospark device was about 1000 A/cm^2 on the basis of the peak electron beam current of 120 A and the anode inner diameter of 4 mm.

4. Conclusion

We fabricated a 10-gap pseudospark device and investigated the electron beam characteristics produced from the device in a pulse charge mode. In the pulse charge mode, pulsed high voltage was applied to the device. We could obtain wide ranges of operating voltage and pressure that could not be obtained in other modes. The wide controllability of voltage and pressure was possible due to the delay time of discharge formation. The discharge delay time decreased from about 10 μs at 5×10^{-2} mbar to about 0.1 μs at 1.0 mbar of Ar. The discharge delay time had a strong dependence on internal gas pressure and a weak dependence on pulse charge voltage. The electron beam diameter was measured and was in the range from 0.1 mm to 4 mm as the internal gas pressure changed from 1.5×10^{-1} mbar to 7×10^{-1} mbar of Ar. The beam diameter was minimum at 3×10^{-1} mbar of Ar, and the beam was well focused. In addition, the electron beam was a maximum of 130 A under this pressure condition. We found another high peak beam current at 3 mbar, but the beam was blurred and thus had a large beam size. The measured FWHM of the beam ranged from 7 to 70 ns. We obtained a maximum power density of 10^{10} W/cm^2 with the multigap pseudospark device in the pulse charge mode. The power density was comparable to that of excimer lasers in a PLD system, but the cost, size, and simplicity of the pseudospark system were much more favorable than those of the PLD system. The pulse-charge-mode multigap pseudospark device could be used as an intense electron beam source in thin film production, material processing, and many other applications.

Acknowledgements

The authors would like to thank Dr. H. Heo for careful reading of the manuscript and valuable discussions, and also Dr. H. S. Kang for giving advice concerning the measurement of beam diameter. They also wish to acknowledge Mr. S. H. Kim and Mr. J. S. Lee for assistance in the experiment.

1) J. Christiansen and C. Schultheiß: Z. Phys. A **290** (1979) 35.
2) J. Christiansen and W. Hartmann: *Gas Discharge Closing Switches*, eds. G. Schaefer, M. Kristiansen, A. Guenther (Plenum, New York, 1990) p. 509.
3) R. B. Miller: *An Introduction to the Physics of Intense Charged Particle Beams* (Plenum, New York, 1982).
4) T. C. Marshall: *Free Electron Lasers* (Collier Macmillan Publishers, London, 1985) p. 18.
5) J. Christiansen: Opt. Commun. **56** (1985) 39.
6) P. Roehlen: Masters thesis, University of Duesseldorf (1985).
7) H. P. Scholch, P. Fickenscher, T. Redel, M. Stetter and G. Saemann-Ischenko: Appl. Phys. A **48** (1989) 397.
8) S. V. Lebedev, M. Machida, S. A. Moshkalyov and D. O. Campos: IEEE Trans. Plasma Sci. **25** (1997) 754.
9) D. L. Pappas, K. L. Saenger, J. Bruley, W. Krakow, J. J. Cuomo, T. Gu and R. W. Collins: J. Appl. Phys. **71** (1992) 5675.
10) K. Frank: 8th Int. Pulsed Power Conf., 1991 p. 472.
11) J. Christiansen: *Physics and Applications of Pseudosparks*, eds. M. A. Gundersen and G. Schaefer (Plenum, New York, 1990) p. 1.
12) D. Bloess, I. Kamber, H. Riege, G. Bittner and V. Brucker: Nucl. Instrum. Methods **502** (1983) 173.
13) R. Stark, O. Almen, J. Christiansen, K. Frank, W. Hartmann and M. Stetter: IEEE Trans. Plasma Sci. **23** (1995) 294.
14) R. Stark, J. Christiansen, K. Frank, F. Mucke and M. Stetter: IEEE Trans. Plasma Sci. **23** (1995) 258.
15) M. Stetter, P. Felsner, J. Christiansen, K. Frank, A. Gortler, G, Hintz, T. Mehr, R. Stark and R. Tkotz: IEEE Trans. Plasma Sci. **23** (1995) 283.
16) W. Benker, J. Christiansen, K. Frank, H. Gundel and W. Hartmann: IEEE Trans. Plasma Sci. **17** (1989) 754.
17) L. C. Pitchford: J. Appl. Phys. **75** (1994) 7227.
18) Y. J. Han: Doctor Thesis, Kyungpook National University (2000).
19) C. J. Liu and M. J. Rhee: IEEE Trans. Plasma Sci. **23** (1995) 235.
20) K. Wille: *The Physics of Particle Accelerators* (Oxford University, New York, 2000) p. 81.